MODELLING THE BEHAVIOUR OF STEEL-FIBRE REINFORCED CONCRETE GROUND SLABS II: DEVELOPMENT OF SLAB MODEL

W. A. Elsaigh, E. P. Kearsley, and J. M. Robberts

Pretoria University

Abstract

Steel Fibre Reinforced Concrete (SFRC) brings favourable properties to concrete pavements. The use of the material is limited by the lack of an appropriate analysis method. This paper is the second in a series of two aimed at providing a modelling approach, which can be used to model the behaviour of SFRC concrete and SFRC ground slabs. In this paper, a finite element model, capable of simulating the non-linear behaviour of the SFRC slab is proposed and compared to the slab's experimental response. An approximate model describing the behaviour of the support layers is developed using results from a plate-bearing test. The same support model is adopted for the analysis of the combined structure of the slab and the support. The material model developed and tested in the first paper, for the SFRC containing 15 kg/m^3 of steel fibres, is adopted for the analysis of the SFRC slabs. In addition, a parameter study is conducted to investigate the influence of concrete strength, steel fibre content and the support stiffness on the *P-Δ* response of SFRC ground slabs.

Corresponding author	Mr. W. A. Elsaigh,	Tel: +27 12 420 4129	walied.elsaigh@uc.edu or whelsaigh@yahoo.com
Co-author	Dr. J. M. Robberts	Tel: +27 12 641 1436	john.robberts@pbmr.co.za
Co-author	Prof. E. P. Kearsley	Tel: +27 12 420 2176	elsabe.kearsley@~~eng.~~up.ac.za

Introduction

Steel Fibre Reinforced Concrete (SFRC) is a composite material consisting of a concrete matrix containing a random dispersion of steel fibres. Addition of steel fibres to concrete improves the engineering properties of the composite material by controlling the crack propagation and widening after crack initiation, allowing the SFRC to absorb large amounts of energy, i.e., indirectly assessed as post-cracking strength, before it collapses. Improved engineering properties of SFRC make the material viable for concrete pavements applications. Indeed, full-scale static testing of centrally loaded ground slabs has demonstrated that the addition of steel fibres increases the load carrying capacity (Beckett, 1990; Falkner et al., 1995a; Bischoff et al., 1996; and Chen 2004). In addition, SFRC pavements under in-service traffic were found to provide superior performance compared to plain concrete as it allows reduction in the slab thickness and yet provide equivalent performance (Elsaigh et al., 2005).

The use of steel fibres in concrete ground slabs allows larger joint spacing (Parker and Rice, 1977) and less maintenance with longer intervals leading to less interruption to traffic (Vandewalle, 1990). Compared to conventionally reinforced concrete pavements, SFRC pavements were found to provide equivalent performance when equivalent amounts of reinforcement are used (Bischoff et al., 2003). In addition, use of SFRC in pavements offers reduced construction time, as the steel fibres are added as one of the concrete mix constituents, and no steel fixing or adjustment is required. Moreover, the presence of steel fibres provides multi-directional reinforcement throughout the thickness of the slab. This is useful as it not only prevent the breaking off at edges where conventional reinforcement is not present (Grondziel, 1989) but also results in a slab section that is reinforced against both hogging and sagging actions. Field investigations have shown that SFRC has much greater spalling endurance compared to plain concrete (Lankard and Newell, 1984). Although the benefits from using SFRC in concrete pavements are reasonably established, the analysis of SFRC pavements is less known as numerical models for analysing SFRC ground slabs are either scarce or do not exist.

The thickness design of concrete ground slabs is the same as for other engineered structures where the aim is to find the optimum thickness that will result in minimal cost and adequate performance. Numerical models developed to analyse plain concrete ground slabs may not be

applied to SFRC as they ignore its post cracking strength contribution to the load carrying capacity of the slab. In fact, steel fibres mainly become active after cracking of the concrete matrix, which means that the un-cracked analysis is not appropriate. Design formulae based on the yield-line theory provided an improved approximation, but still underestimate, of the ultimate load when compared to the elastic theory approach, such as models developed by Meyerhof (1962), Losberg (1978) and Rao and Singh (1986). If we are to seek a greater exploitation of SFRC, analysis should proceed beyond the initial cracking point. Recently, non-linear finite element methods were implemented to analyse SFRC ground slabs with different levels of success (Falkner et al. 1995b, Barros and Figueiras, 2001 and Meda and Plizzari, 2004). Accuracy of non-linear finite element analysis methods is much dependent on the appropriateness of the material constitutive model and the representation of the cracks.

This is a second paper in a series of two focusing on nonlinear modelling aspects of SFRC ground slabs. In the first paper, the material model was derived and utilised in analysing SFRC beam. The determined σ-ε response along with the experience and results obtained from the non-linear finite element analysis of the beam is utilised in analysing SFRC ground slab manufactured using similar material as in the beam. The main objectives of this paper are: (a) propose a finite element model, capable of simulating the non-linear behaviour of the SFRC ground slabs and (b) investigate the effect of the SFRC strength, steel fibre content, support stiffness and slab thickness on the load-displacement response (P-Δ) response, thereby, optimising these parameters in order to obtain a desired load carrying capacity and examine the possibility of ultra-thin SFRC slabs.

Physical model

The full-scale SFRC ground slab tested by Elsaigh (2001) is utilised for the purpose of this analysis. The slab dimensions and supporting layers are presented in Figure 1. The SFRC slab is manufactured using similar material as that in the beam discussed in the first paper.The foamed concrete support was chosen because it can readily be moulded and kept bound until the end of the experiment. The slabs were cast in a shaded area and were covered by plastic sheets for 28 days before the tests were conducted. Testing was conducted using a closed-loop testing system applying displacement at a rate of 1.5 mm/min. The load was applied using a hydraulic twin jack

pressing on a stiffened loading plate (100 x 100 mm). The vertical displacements were measured by using Linear Variable Displacement Transducers (LVDT) mounted on a steel beam spanning over the tested slabs. In addition, a plate loading test was performed on the surface of the foamed concrete slab to establish the *P-Δ* of the supporting material. A circular steel plate with a diameter of 250 mm and a thickness of 40 mm was used in the test.

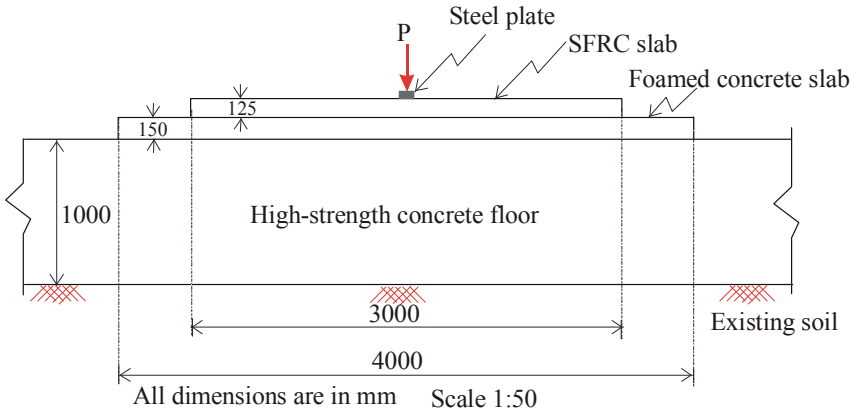

Figure 1: Layout of the slab test.

Support layers model

The aim of this section is to develop an approximate model that describes behaviour of the support layers below the SFRC slab. The support layers are reduced to a single representative slab having the dimensions of the foamed concrete slab. The foamed concrete slab is assumed to rest on a rigid bed since the deformations within the 1000 mm deep, high strength, concrete floor are expected to be insignificant compared to the deformations within the SFRC and foamed concrete slabs.

Due to symmetry, only a quarter of the foamed concrete slab is modelled. An equivalent square loading plate, measuring 110 x 110 x 40 mm, is assumed instead of the circular plate used in the experiment. This is to simplify the geometry and thus reduce the calculation required for the finite element analysis. Element type 7 of MSC.Marc (2003), a three-dimensional, first order eight-node element, is prescribed for the analysis. The stiffness of the element is formed using eight-point Gaussian integration. A node in this element has three degrees of freedom; those are

displacements in X, Y and Z directions (Δ_X, Δ_Y and Δ_Z). A quarter of the foamed concrete slab is approximated by a finite element mesh consisting of 450 elements while a single element is used for the steel plate. Two layers of 75 mm each were specified for the foamed concrete slab. The displacement of all the nodes at the bottom of the slab is constrained in the Z-direction. The displacements for the nodes at the symmetry planes X = 0 and Y = 0 were constrained in the X-direction and the Y-direction respectively. The displacement-controlled loading is simulated by increasing the displacement from zero to -10 mm using the "time curve concept" available in the MSC.Marc.

A trail-and-error procedure is followed to generate the material model for the foamed concrete slab. In the beginning, linear elastic compressive stress-strain (σ-ε) response is assumed, as in Figure 2a. The value of the Young's modulus is changed until the first parts of the calculated and experimental *P*-Δ responses are matched. A value of 130 MPa and 0.05 was adopted for the Young's modulus and Poisson's ratio respectively. The adopted Young's modulus falls within the range of values suggested by the American Concrete Institute Committee (2000). In the next step a post-yielding part is added to the σ-ε response. The post-yielding part was adjusted following the sequence in Figure 2 (b), (c), (d) and (e) until the entire calculated and experimental *P*-Δ responses are matched as shown in Figure 3.

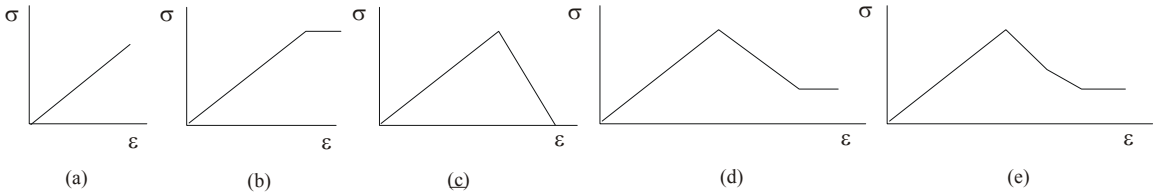

Figure 2: Steps followed to generate the stress-strain response for the foamed concrete support.

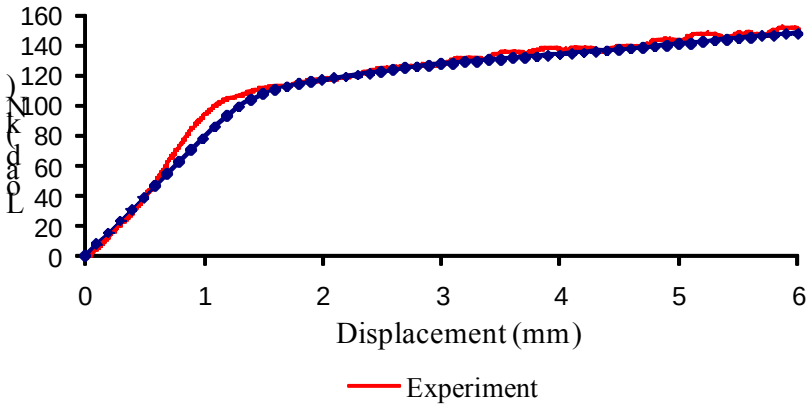

Figure 3: Computed and measured load-displacement responses for plate-bearing test.

Idealisation of the SFRC ground slab

Because of symmetry, only a quarter of the slab is analysed. Element type 75 of MSC.Marc (2003) is used. It is a four-node thick shell element with six degrees of freedom per node those are three displacements (Δ_X, Δ_Y and Δ_Z) and three rotations (θ_X, θ_Y and θ_Z). The stiffness of this element is formed using four-point Gaussian integration. It has bending, membrane and transverse shear capabilities which suites the ground slabs applications. Based on the experience gained from the SFRC beam analysis, the thickness of the slab is divided into eleven layers (density of integration points through the thickness equals eleven). A single shell element of type 75 is used for the square loading plate. The displacement of the nodes of the SFRC slab and the loading plate at the symmetry planes X = 0 and Y = 0 were constrained in the X-direction and the Y-direction respectively (refer to Figure 4).

The size of the element used to model the SFRC slab is chosen to be 150 x 150 mm analogous to the size of the element used when developing the material model for the SFRC. The same tensile σ-ε response is applied to the elements having a width of 75 mm. This is because only quarter of the slab is modelled and therefore half of the fracture energy will be dissipated while cracking occurs in one strip of elements on the centre line through the middle of two opposite edges. The same is assumed for the other strip of elements perpendicular to the first one. In other words only half of the crack is modelled when selecting quarter of the slab model. The two trapezium elements and the 50 x 50 mm element (as indicated in Figure 4) were necessary in order to adapt

the mesh to the size of the loading plate. The post-cracking part of the tensile σ-ε response therefore needs to be modified for these three elements. Larger element sizes were used for elements away from expected crack path and are expected to have insignificant influence on the *P-Δ* response for a slab loaded at its centre. The nodes of the loading plate are tied to the relevant element (50 x 50 mm) in the SFRC slab. Through this tying, all the displacements and rotations of the SFRC for the particular slab element are set to be dependent on the corresponding nodes of the loading plate.

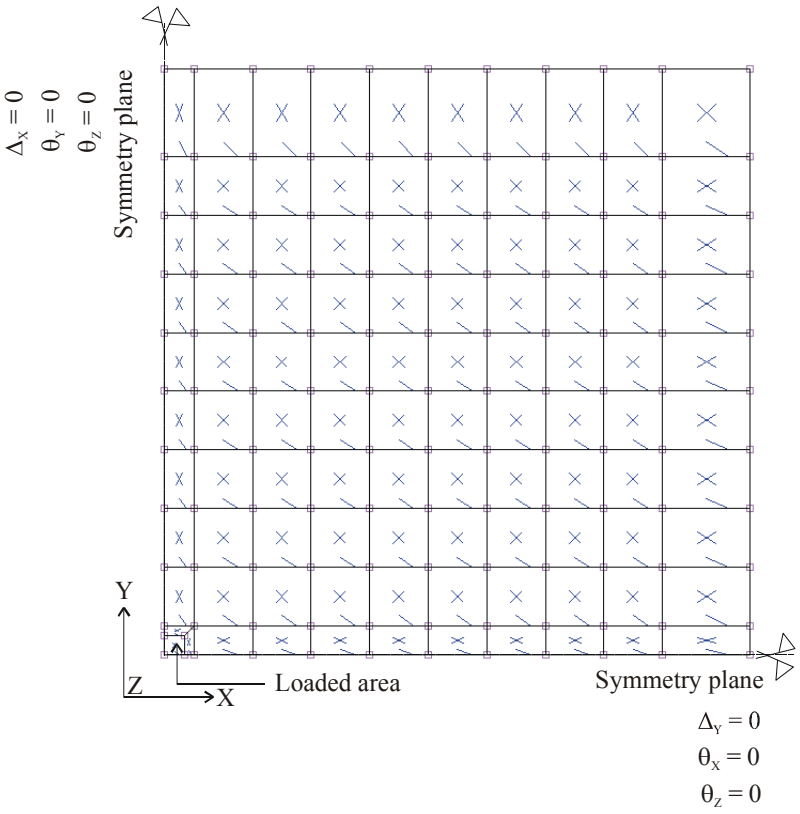

Figure 4: The mesh and the boundary conditions for the SFRC slab.

The contact between the SFRC slab and the foamed concrete slab was represented by two deformable friction contact bodies with touching contact. Touching contact means that two deformable bodies can either be in contact or can be separated. If a node is found to be in contact, the node is constrained in the direction normal and tangential to the contact body. Separation occurs when the tensile contact normal stress on a node in contact becomes larger

than the separation threshold stress. The contact is useful to connect independently meshed parts of a structure or to connect two parts of a structure where different types of elements are used (i.e. to connect shell elements and brick elements).

Two contact bodies are specified separately for the SFRC slab and the foamed concrete slab. Initially, the SFRC slab is set to be in contact with the foamed concrete slab. At a particular node, the SFRC slab loses contact with the foamed concrete slab when the tensile stress reaches 0.01 MPa. The specified value for separation stress (0.01MPa) was decided upon by performing several runs in the model. A friction factor of 0.1 was assumed between the two contact surfaces. The validity of the assumptions regarding separation tensile stress and friction stress is justified through a sensitivity study presented in Elsaigh (2007).

Material model for the SFRC slab

The analyses conducted in this research involve biaxial tension and biaxial compression stress states in slabs. These stress states is modelled by combining crack detection surfaces and compression yield criterion to limit the tensile cracking and compressive yielding respectively. The maximum principal stress criterion of Rankine is used. According to this criterion, brittle fracture of concrete takes place when the maximum principal stress at a point inside the material reaches a value equal to the tensile strength of the material regardless of the normal or shearing stresses that occur on other planes through the point. This fracture surface is referred to as the fracture cut-off surface or tension-failure surface or simply tension cut-off (Chen, 1982). The yield of concrete is described by Drucker-Prager yield criterion.

The uniaxial σ-ε response presented in Figure 5, developed from the beam analysis for the same slab concrete, is prescribed for this analysis. The validity using a uniaxial tensile σ-ε response to describe ~~a~~ biaxial bending is justified by Kupfer (1969) suggesting that, under biaxial tension, the strength is almost the same as that of uniaxial tensile strength. In other words, the controlling biaxial tensile stress is almost independent of the stress ratio (Chen, 1982).

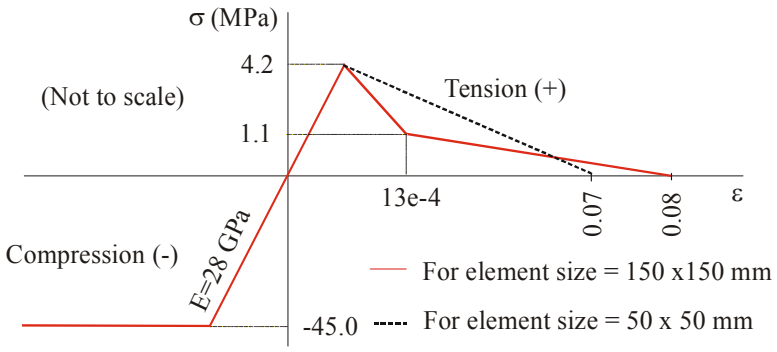

Figure 5: The stress-strain response for SFRC containing 15 kg/m^3.

The tensile σ-ε response is adjusted for finite elements smaller than 150 x 150 mm. The adjustment is made for the post-cracking part of the curve based on fracture energy. The dotted line in Figure 5 represents the softening response used for the 50 x 50 mm and the trapezium elements. A linear softening response is used for these elements because MSC.Marc (2003) only allows for the input of a single cracking subroutine, which was reserved for elements measuring 150 x 150 mm. The slope for the dotted line of Figure 5 is determined by keeping the fracture energy unchanged. The fracture energy can be calculated as the product of the area ($A_{150x150}$) under the softening part of the tensile σ-ε response and the crack smearing width as indicated in equation 1:

$$G_f = 150.A_{150x150} \qquad (1)$$

If the crack smearing width is changed to 100 mm, the area ($A_{100x100}$) under the softening part of the tensile σ-ε response can be calculated as indicated in equation 2:

$$A_{100\,x100} = \frac{G_f}{100}. \qquad (2)$$

The $A_{100x100}$ can be used to determine the ultimate strain and therefore the slope of the linear softening part for the tensile σ-ε response of an element with a width of 100 mm. The same procedure can be followed to calculate the slope of the linear softening part for an element with a width of 50 mm.

Results of the finite element analysis of the SFRC ground slab

Figure 6 shows the correlation between the calculated and the experimental *P-Δ* responses. The calculated *P-Δ* response is generated by plotting the vertical displacement and four times the reactions at the loading node resulted from consecutive increments. The calculated and the experimental *P-Δ* responses reasonably match up to a vertical displacement of approximately 3 mm. The calculated *P-Δ* response deviates significantly from the experimental response beyond this value. The load drop (after increment 256) coincides to the extension of the bottom crack from the centre of the slab to the centre of the edges. The calculated *P-Δ* response beyond increment 256 is unrealistic and should be discarded.

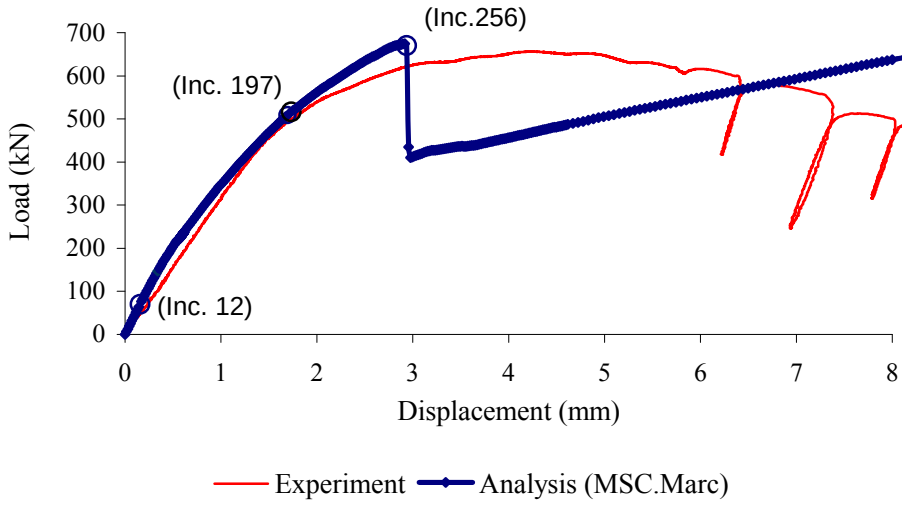

Figure 6: Computed and measured load-displacement responses for the SFRC ground slab.

The analysis conducted here provided an improved estimation for the load-carrying capacity of the SFRC slab compared to existing theories usually used in for designing such slabs. For example, the maximum load calculated for this slab using Meyerhof formulae is approximately 211 kN which is almost three times less than the actual load (650 kN). A valuable advantage of the developed non-linear finite element model is that it provides the magnitude of displacement, the extent of the crack and the tensile stress level for each load point on the *P-Δ* response.

The progress of cracking, on the top and bottom of the SFRC slab, during the loading process is shown in Figure 7. The crack evolution indicates that stress redistribution took place after the initial crack occurred in the SFRC slab. The post-cracking strength of the SFRC seems to have played a significant role in redistributing these stresses eventually increasing the load carrying capacity of the slab. In fact, statically determinate structures such as simply supported beams benefit little from the advantage of using SFRC as its load carrying capacity reduces after cracking, whereas, statically indeterminate structures such as ground slabs benefits the utmost due to formation of plastic hinges accompanied by stress redistribution (Nemegeer, 1996). The stress redistribution can also be recognised from the ductile behaviour of the SFRC shown in Figure 6. The ability of ductile slab to sustain the maximum load would therefore not necessarily imply failure at first cracking. To these ends, the primary motivation for using steel fibres in ground slabs is not only the increase of the SFRC modulus of rupture but also increase the amount of energy that can be absorbed before collapse (i.e., the post cracking strength of SFRC).

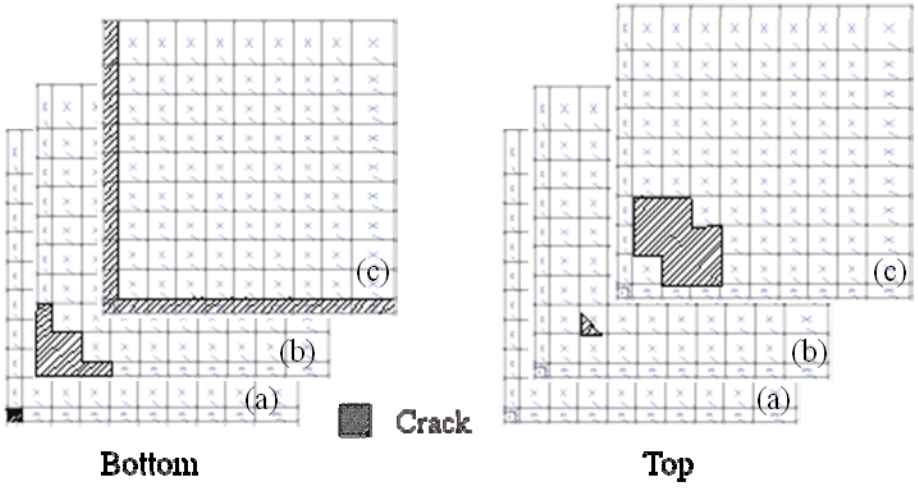

Figure 7: The progress of cracking in the SFRC slab.

Parameter study on SFRC ground slabs

A parameter study is conducted to investigate the influence of concrete strength, steel fibre content, support stiffness and SFRC slab thickness on the *P-Δ* response of SFRC ground slabs.

In the analysis, only one parameter will be changed at a time while keeping the other parameters fixed.

Hypothetical SFRC slabs measuring 3000 x 3000 x 100 mm are assumed except for the last two analyses where the slab thickness is reduced to 50 mm in order to investigate the possibility of ultra-thin slabs. The support was made of typical pavement materials with its depth kept unchanged for all the analyses. Table 1 shows the various support materials used in the performed analyses. The codes C2, G5, G6 and G9 follow the South African classification for road building materials. The values in Table 1 are either estimated or adapted from the study conducted by Theyse et al. (1996). The cohesion and the angle of friction served as inputs to the Drucker-Prager criterion used for the support material. Poisson's ratio was assumed to be 0.35 for all the support materials used here.

Table 1: Materials used for the support layer.

Classification	Young's modulus (MPa)	Cohesion (MPa)	Angle of internal friction
C2	500 MPa	0.223(*)	5.50 (*)
G5	250 MPa	0.143	3.60
G6	150 MPa	0.103	2.88
G9	50 MPa	0.1(*)	1.60 (*)

(*) Estimated values

The SFRC slabs were centrally loaded by using a steel plate measuring 75 x 75 mm. The size of the loading plate is chosen so that the quarter of the plate fits the size of the finite elements on the symmetry planes. This is to avoid the complexities related to the use of trapezium and the smaller elements when adapting the finite element mesh to the size of the loading plate. The finite element mesh and the boundary conditions for quarter of the hypothetical slab were kept unchanged for all the analyses.

Effect of changing strength of concrete

Figure 8 shows two tensile σ-ε curves for SFRC where only the tensile and compressive strengths are changed. Changing the strength of concrete influences the Young's modulus and the elastic strain. Only the effect due to the change in the Young's modulus is studied here. The possible change in the value of the cracking strain is deemed to be limited and therefore not considered. The increase in the strength of the concrete is expected to increase the post-cracking strength. For the purpose of this analysis, this effect the concrete strength is assumed to be limited only to the first part of the softening curve in the σ-ε response. For the support, G9 material is used.

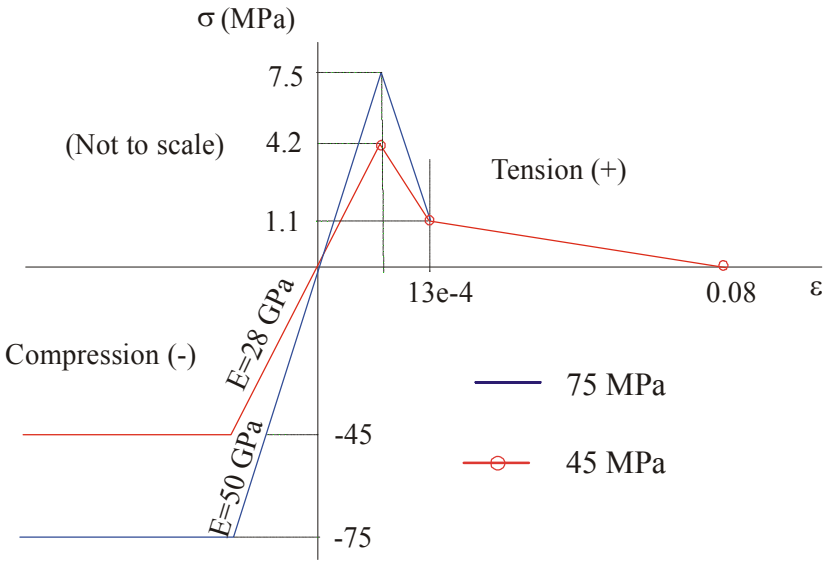

Figure 8: Stress-strain curves - changing strength of SFRC.

Figure 9 shows that an increase in tensile and compressive strength, results in an increase in the load carrying capacity of the SFRC ground slabs. For example, at a displacement of 4 mm in the *P-Δ* responses, the load is increased by approximately 39 percent due to an increase of 67 percent in the strength of the concrete (from 45 MPa to 75 MPa). The improvement in the load-carrying capacity is greater at higher displacements than for lower displacements. It also reduces the vertical displacements for equal loads, consequently, reducing support erosion potential often associated with thin concrete pavements.

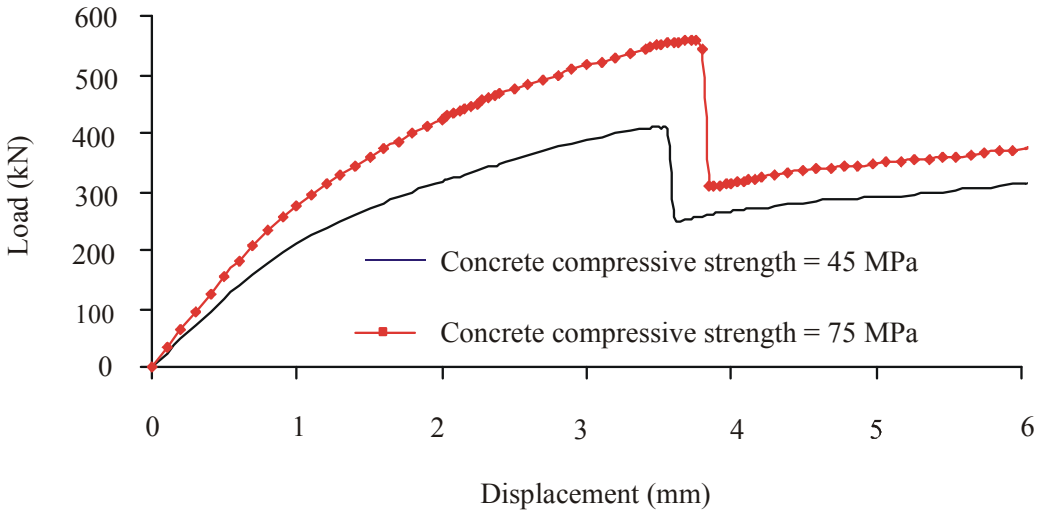

Figure 9: Effect of changing strength on load-displacement responses.

Effect of changing steel fibre content

Changing the steel fibre content largely results in changing the post-cracking strength of the SFRC. This influences the slopes of the softening part of the tensile σ-ε curve. Figure 10 shows the σ-ε responses used in the analysis. For the support, G9 material is used. The σ-ε response representing the 45 MPa SFRC is similar to the model calculated for SFRC containing 15 kg/m^3 of steel fibres. The σ-ε response for approximately 65 kg/m^3 of similar steel fibres is estimated based on the trends shown in the steel fibre manufactures design tables (Bekaert, 1999).

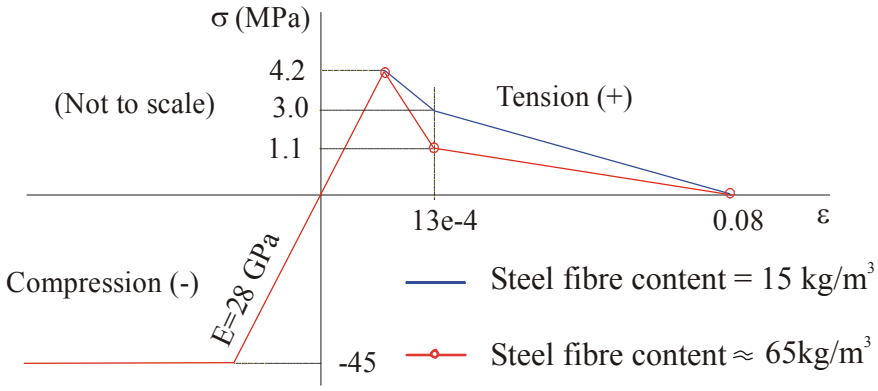

Figure 10: Stress-strain curves for SFRC - changing the steel fibre content.

Figure 11 indicates that increasing the steel fibre content increases the load-carrying capacity of the SFRC ground slab. It also improves the ductility of the SFRC slab. The SFRC slab with a higher steel fibre content sustained the maximum load for greater displacement values. The analysis showed that the increase in the load-carrying capacity, due the increase in steel fibre content, is significant. At a deflection of approximately 3.5 mm, the addition of extra steel fibres results in approximately 21 percent improvement in the load-carrying capacity. The increase in the percentage of the steel fibre content does not mean an increase of similar percentage in the load carrying capacity of the SFRC slab. However, the presence of the steel fibres in ground slabs was shown to increase the load-carrying capacity compared to plain concrete slabs. This was demonstrated by many full-scale experiments comparing SFRC and plain concrete ground slabs.

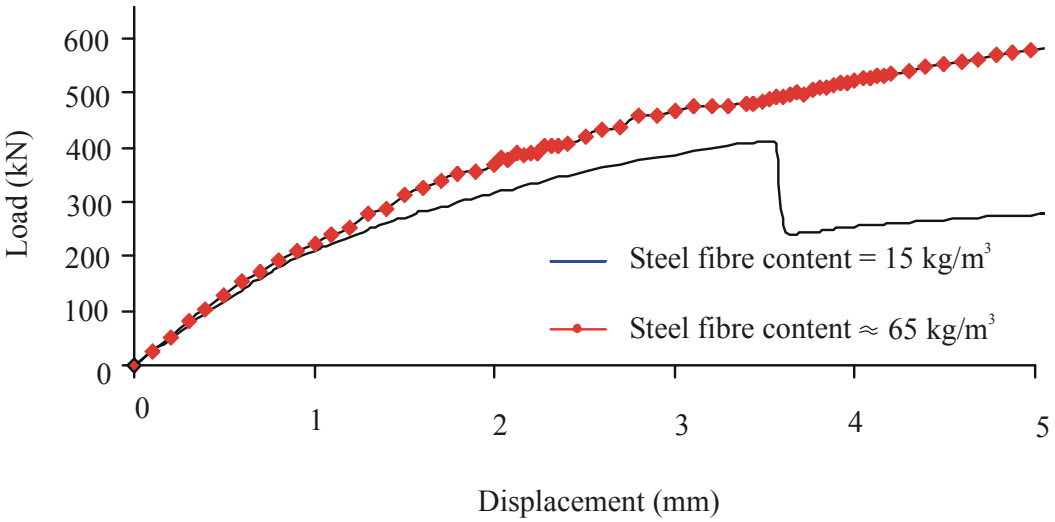

Figure 11: Effect of changing steel fibre content on the load-displacement responses.

It is worth noting that the steel fibre content and concrete matrix strength are interconnected with respect to their influence on the P-δ response and post-cracking strength. Elsaigh and Kearsley (2006) suggested that for every concrete compressive strength, a range of useful steel fibre contents exists. Steel fibre content falling out of this range will have no or little contribution to the post-cracking strength of SFRC. Within the range of the useful steel fibre contents, an increase in steel fibre content will result in an increase in the post-racking strength.

The upper limit of the useful range of steel fibre content, i.e., optimum steel fibre content, differs for different types of steel fibres and different concrete strength. In view of that, utmost benefit from SFRC in ground slab is obtainable only by balancing the steel fibre content and the concrete compressive strength.

Effect of changing support stiffness

The support materials G6 and G9 were used in the analysis. The material model for the SFRC containing 15 kg/m^3 was used and kept unchanged.

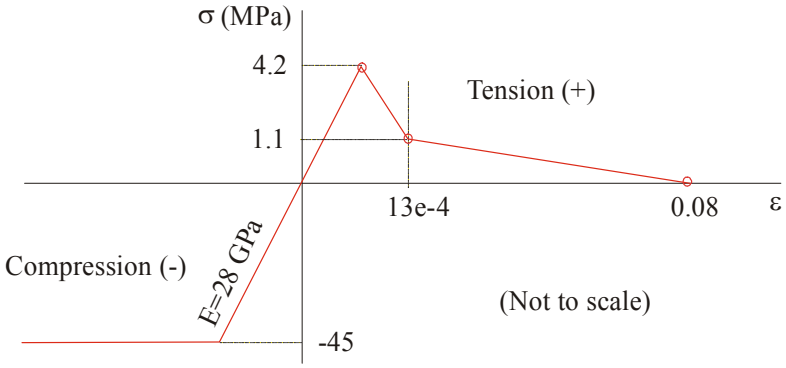

Figure 12: Stress-strain curves for SFRC used to study the effect of the support stiffness.

Figure 13 indicates that increasing the support stiffness significantly increases the load-carrying capacity of the SFRC ground slab. It also reduces vertical displacements for equal loads. For example, at a displacement of approximately 4 mm in the *P-Δ* responses, the load is increased by approximately 30 percent due to an increase of three times in the stiffness of the support (Young's modulus increased from 50 MPa to 150 MPa). This is similar in trends to the effect obtained by increasing the strength of the SFRC. However, increasing the strength of the SFRC is found to provide higher load-carrying capacity compared to increasing the support stiffness.

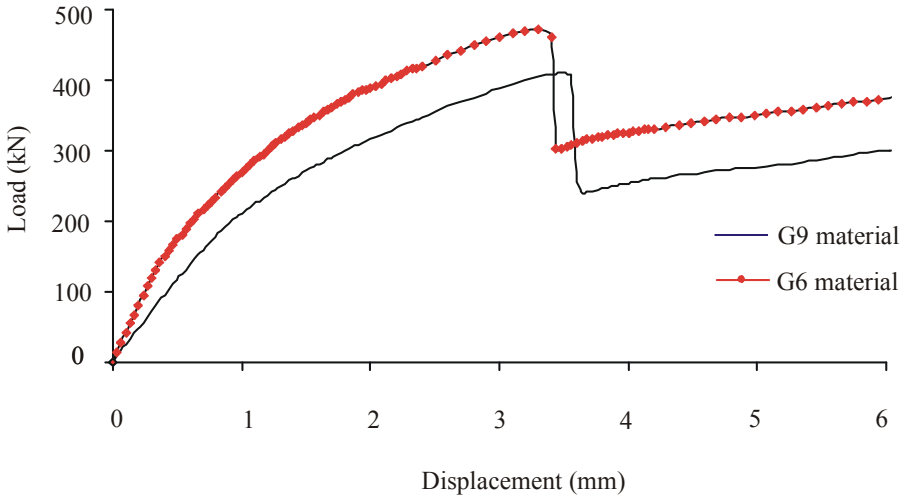

Figure 13: Effect of changing support stiffness on the load-displacement responses.

Effect of slab thickness

Based on the trends shown earlier with respect to the effect of the various parameters on the P-Δ response, a potential for ultra-thin SFRC pavements exists. Two support materials, i.e., C2 and G5, and two SFRC materials were used. Figure 14 shows the σ-ε responses assumed for the analysis. Both σ-ε curves represent an assumed SFRC made of high strength concrete and contain high steel fibre content. The Young's modulus of the SFRC is fairly estimated based on the cube strength of concrete (Holcim Material Handbook, 2006). The cracking strength is assumed as 10 percent of the cube strength. The residual strength is estimated as 90 percent of cracking strength based on design tables provided by steel fibre manufactures (Bekaert, 1999). The thickness of the SFRC is arbitrarily chosen to be 50 mm.

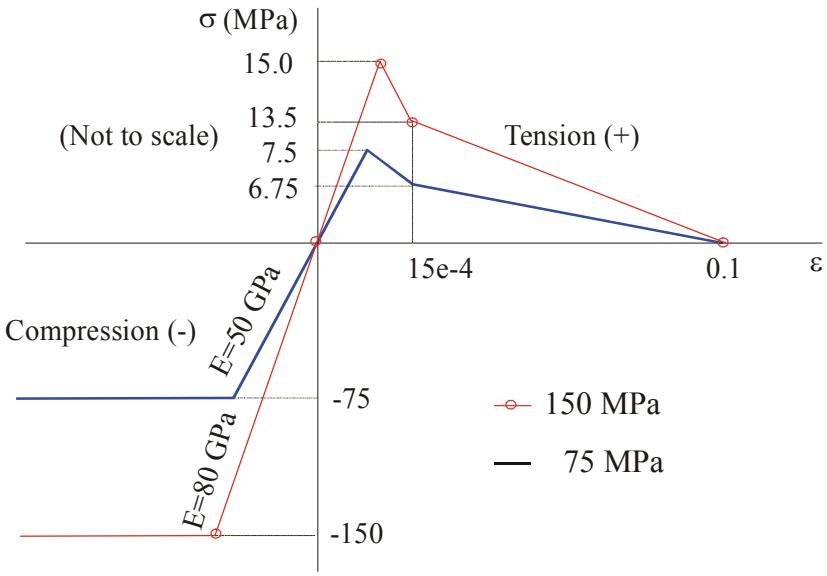

Figure 14: Stress-strain curves for SFRC used to study the effect of slab thickness.

Figure 15 shows the *P-Δ* responses calculated for a relatively thin SFRC ground slab. Comparing Figure 15a and b, the load-carrying capacity of a 50 mm thick SFRC slab can be increased by approximately three times by doubling the strength of the concrete, the support stiffness and using a high steel fibre content. The influence of the support stiffness is greater for higher strength concrete than for lower strength concrete. The trends shown here indicate that ultra-thin slabs can be designed by manipulating the strength of concrete, the steel fibre content and the support stiffness. The appropriate steel fibre content for a particular high strength concrete will need to be a subject for further research.

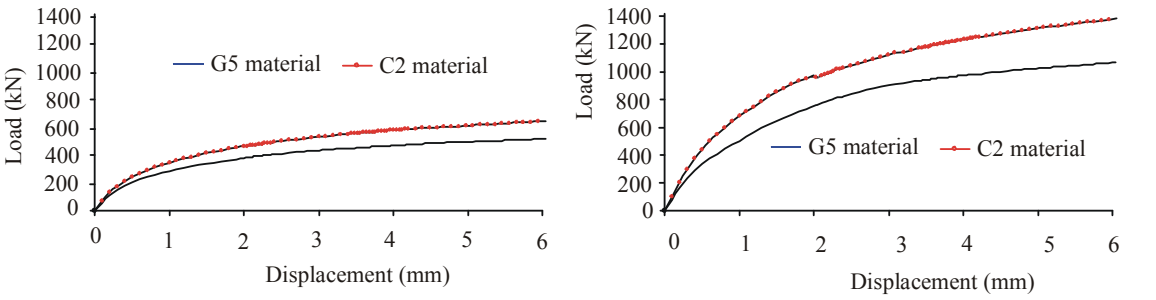

(a) Concrete compressive strength = 75 MPa

(b) Concrete compressive strength = 150 MPa

Figure 15: The load-displacement responses for thin SFRC ground slabs.

Summary and conclusions

The calculated tensile σ-ε response and the developed finite element model for SFRC slabs can be used to satisfactorily model the behaviour of SFRC ground slabs subjected to interior loading. The uniaxial σ-ε response calculated using the developed numerical method was found sufficient for modelling the biaxial bending response of the analysed SFRC slabs. Thus the assumption that "a crack in a particular direction does not influence the tensile strength of the material parallel to the crack direction" seems to be valid. Further experiments are required to investigate its validity of the developed approach for the edge and corner load cases.

A valuable advantage of the developed non-linear finite element analysis is its capability of providing the magnitude of displacement, the extent of the crack in the top and bottom of the slab, and the tensile stress for each load point on the P-Δ response. Availability of such information may enable and encourage the move towards implementation of limit-state philosophy in pavement design. Possibility of adopting such a design philosophy will continue to be a challenging aspect in the future due to inadequacy in the current available methods which are based on transfer functions derived using statistical analysis.

Increasing the strength of concrete and the steel fibre content increases the load-carrying capacity of the SFRC ground slabs. The increase due to concrete strength is larger than the increase due to steel fibre content. The influence of the steel fibre content is not only dependent on the steel fibre parameters but also dependent on the strength of concrete. An optimum steel fibre content exists for different concrete strengths, thereby, a balance has to be made between these two parameters to obtain the utmost.

Increasing the support stiffness increases the load carrying capacity of the SFRC ground slabs. The increase is higher for greater strength concrete than for lower strength concrete. Increasing the strength of concrete results in a larger increase in the load-carrying capacity compared to increasing the support stiffness.

Theoretically an ultra-thin SFRC ground slab can be designed. This can be achieved by providing a relatively hard support, using high strength concrete and optimum steel fibre content. An economic design can be worked out by manipulating these three components.

Notation

The following symbols are used in this paper:

A	=	Area of beam cross-section.
E_c	=	Young's modulus for of the SFRC.
P	=	Vertical load.
X , Y, and Z	=	Orthogonal directions.
Δ_X, Δ_Y and Δ_Z	=	Displacement in the X, Y, and Z directions respectively.
θ_X, θ_Y and θ_Z	=	Rotation in the X, Y and Z directions respectively.
σ	=	Stress.
ε	=	Strain.
δ	=	Deflection of elevated beam.
Δ	=	Deflection of ground slab.

References

American Concrete Institute Committee 523 (2000). Guide for Cast-in-Place Low Density Concrete. ACI Manual of Concrete Practice: Part 5. ACI 523. IR-92. 8P.

Barros, J.A.O., and Figuieras, J.A. (2001). Model for the Analysis of Steel Fibre Reinforced Concrete Slabs on Grade. Journal of Computers & structures (79). PP 97-106.

Beckett, D. (1999). Corner and Edge Loading on Concrete Industrial Ground Floors Reinforced with Steel Fibres. Concrete, V. 33, No. 3. PP 22-24.

Bekaert, (1999). Steel Fibers for the Pre-cast Industry. Bekaert NV. Dramix Technical Pamphlet.

Bischoff, P.H., Valsangkar, A.J., and Irving, J.A. (1996). Experimental Study of Concrete Floor Slabs on Grade. Proceedings of the Canadian Society for Civil Engineering Annual Conference, V. IIa, Monterial / Canada. PP 273-282.

Bischoff, P.H., Valsangkar, A.J., and Irving, J. (2003). "Use of Fibres and Welded-Wire Reinforcement in Construction of Slabs on Ground". Practice Periodical on Structural Design and Construction, V. 8, No. 1, ASCE, ISSN 1084-0680. PP 41-46.

Chen, S. (2004). Strength of Steel Fibre Reinforced Concrete Ground Slabs. Proceedings of the Institution of Civil Engineers, Structures& Buildings 157, Issue SB2. PP 157-163.

Chen, W.F. (1982). "Plasticity in Reinforced Concrete". McGraw-Hill, New York / United States of America, 1st edition.

Elsaigh, W.A. (2001). "Steel Fibre Reinforced Concrete Ground Slabs". M.Eng. Dissertation, University of Pretoria / South Africa.

Elsaigh, W.A., Kearsley, E.P., and Robberts, J.M. (2005). "Steel Fibre Reinforced Concrete for Road Pavement Applications". Proceedings of the 24th Annual Southern African Transport Conference, Pretoria / South Africa. 10 P.

Elsaigh, W.A., and Kearsley, E.P. (2006). Effect of Matrix Strength on Performance of Steel Fibre Reinforced Concrete. Proceedings of the 3rd Young Concrete Engineers' Practitioners' and Technologists' Conference, Midrand / South Africa. 10 P.

Elsaigh, W.A. (2007). Modelling the Behaviour of Steel Fibre Reinforced Concrete Ground Slabs. Ph.D. Dissertation, University of Pretoria / South Africa.

Falkner, H., Huang, Z., and Teutsch, M. (1995a). Comparative study of Plain and Steel Fibre Reinforced Industrial Ground Slabs. Concrete International, V. 17, No 1. PP 45-51.

Falkner, H., Huang, Z. and Teutsch, M. (1995b). Untersuchung des Trag-und Verformungsverhaltens von Industriefußböden aus Stahlfaserbeton. Institut Für Baustoffe, Massivbau und Brandschutz (IBMB) / Germany, Heft No. 117, ISBN3-89288-096-4. 187 P. (In German).

Grondziel, M. (1989). "Restoration of Concrete Floors with Steel-Fibre Concrete for Aircraft at Frankfurt Airport". Proceedings of the International Conference on Recent Developments in Fibre Reinforced Cements and Concrete, London / United Kingdom. PP 610-619.

Holcim,(2006). Holcim Material Handbook. Published by Johnson Heydenberg Afrika, Holcim South Africa. 2nd Edition.

Kupfer, H., Hilsdorf, H.K., and Rusch, H. (1969). Behaviour of Concrete Under Biaxial Stresses. Journal of the American Concrete Institute, V. 66, No. 8. PP 656-666.

Lankard, D.R., and Newell, J.K. (1984). Preparation of Highly Reinforced Steel Fibre Reinforced Concrete Composites. Proceedings of the International Symposium, American Concrete Institute, Detroit / United States of America. PP 287-304.

Losberg, A. (1961). Design Methods for Structurally Reinforced Concrete Pavements. PhD. Thesis, Transactions No. 250, Chalmers University of Technology, Gőteborg.

Meda, A., and Plizzari, G.A. (2004). New Design Approach for Steel Fibre-Reinforced Concrete Slab-on-Ground Based on Fracture Mechanics. American Concrete Institute, Structural Journal, V.101, No. 3. PP 298-303.

Meyerhof, G.G. (1962). Load Carrying Capacity of Concrete Pavements. Journal of the Soil Mechanics and Foundations Division, The American Society of Civil Engineers. PP 89-116.

MSC.Marc, (2003). Mentat V. 2003, MSC. Software Corporation, 2 Mac Arthur place, Santa Ana, CA92707. United State of America.

Nemegeer, D. (1996). Design Guidelines for Dramix Steel Wire Fibre Reinforced Concrete. Indian Concrete Journal, V.70, No.10. PP 575-584.

Parker, F.Jr. and Rice, J.L. (1977). Steel Fibrous Concrete for Airport Pavements. Proceedings of the International Conference on Concrete Pavement Design, Purdue University / Unite States of America. PP 541-555.

Rao, K.S.S., and Singh, S. (1986) .Concentrated Load-Carrying Capacity of Concrete Slabs on Ground. ASCE Journal of Structural Engineering, V. 112, No. 12. PP 2628-2645.

Theyse, H.L., De Beer, M., and Rust, F.C. (1996). Overview of the South African Mechanistic Pavement Design Analysis Method. Transportek, CSIR, DP-96/005, Pretoria / South Africa. 43P.

Vandewalle, M. (1990). The Use of Steel Fibre Reinforced Concrete in Heavy Duty Port Pavements. Proceedings of the 6th International Symposium on Concrete Roads: Theme B, Madrid / Spain. PP 121-128.

Section	No. of words	(%)
Introduction	675	8.2
Physical model	448	5.4
Support layers model	925	11.2
Idealisation of SFRC G. Slab	876	10.6
Material model for SFRC G.S	674	8.1
Results of FEA on the slab	895	10.7
Parameter analysis	427	5.2
Effect of changing strength	715	8.6
Effect of changing steel f. Cont.	890	10.8
Effect of changing support stiffness	630	7.6
Effect of slab thickness	750	9.1
Summary and conc.	372	4.5
Total	8277	100